



Admix of $\text{Cu}_2\text{ZnSnS}_4$ and ZnS as thin film to absorb visible light

J. M. Rodríguez-Valencia¹ · S. H. Adendaño-Guin² · L. Rojas-Blanco¹ · G. Pérez-Hernández¹ · O. Sarracino-Martínez³ · I. Zamudio-Torres¹ · R. Castillo-Palomera² · F. Paraguay-Delgado⁴ · Erik R. Morales¹

Received: 2 October 2018 / Accepted: 28 January 2019 / Published online: 7 February 2019
© Springer Science+Business Media, LLC, part of Springer Nature 2019

Abstract

Admix of $\text{Cu}_2\text{ZnSnS}_4$ (CZTS) and ZnS phases in thin films were prepared on glass substrate by thermal evaporation from CuS, ZnS and SnS as precursors. Their composition, microstructure and optical properties of thin films were determined using energy dispersive X-ray spectroscopy (EDS), X-ray diffraction (XRD), scanning electron microscopy (SEM) and UV–Vis absorption. The conglomerate grain shape of the obtained materials are elongated with dense morphology. Kesterite structure was obtained after heat treatment at 400 °C of precursors. By Rietveld refinement method was determined the presence of CZTS phase and ZnS phase at 65% and at 35%, respectively. By elemental analysis, it was noticed Cu loss in the heating process. Band gap value of the resulting material was 1.49 eV. Regarding to the optoelectronic properties for solar cells, this film shows good photoconductivity.

1 Introduction

Photovoltaic materials are made by different processes due to global energy demand. One of them is using binary compounds as precursors to get CZTS with kesterite or wurtzite structure, it is one of the alternatives to get these photovoltaic types of materials. Different methodologies to get adequate material have received an enormous interest by research and industry community. Some of the absorber materials for photovoltaic applications are perovskite, CuInGaS, materials with kesterite structure.

Materials with kesterite structure, is a mineral whose elemental composition could be $\text{Cu}_2\text{ZnSnS}_4$, Cu_2ZnSnSe (CZTSe), and their alloys or dopant $\text{Cu}_2\text{ZnSn}(\text{S}_x\text{Se}_{1-x})_4$,

(CZTSSe). Since the nature of these types of materials are photoactive, they are applied in photocatalysis [1–4]. In addition, it has been reported adequate optoelectronic properties for solar cells applications [5–7]. These properties make them suitable candidates for application in thin film solar cell assembly as absorber material. Further, the CZTS are composed by earth-abundant elements and it is a non-toxic compound. The solar cell assembly using current kesterite has certified a record of 13.8% efficiency, in a small active area device [8].

Different synthesis methodologies to get thin films have been reported. Such as pulsed laser deposition [9], sputtering [10], chemical bath deposition [6], drop coating [11], dip coating [12], Doctor-Blade printing [13], spray pyrolysis [14], solvothermal [15], electrodeposition [16], plasma assisted co-evaporation [17], ink-print method [5] and thermal evaporation [18].

The thermal evaporation technique has good advantage due to its capacity to produce uniform films with adequate adherence. This technique uses to evaporate electric resistive heater, the material source is placed inside the heater boat under high vacuum ($< 8 \times 10^{-6}$ mbar) [19]. At adequate temperature, the source material is dissociated into vapor on the constituent elements, and they travel the distance between the heater boat and the substrate (normally kept directly above the boat) without getting scattered. Once they reach the substrate, each one will settle and get adsorbed on to the substrate surface forming a thin film, according to the

✉ Erik R. Morales
eriking10@hotmail.com

¹ Universidad Juárez Autónoma de Tabasco, Avenida Universidad S/N, Col. Magisterial, C.P. 86040 Villahermosa, Tabasco, Mexico

² Universidad Politécnica de Chiapas, Carretera Tuxtla Gutiérrez - Portillo Zaragoza km 21+500, Colonia Las Brisas, Suchiapa, Chiapas, Mexico

³ Universidad Popular de La Chontalpa, Carretera Cárdenas-Huimanguillo km 2, H. Cárdenas, Tabasco C.P. 86500, Mexico

⁴ Centro de Investigación en Materiales Avanzados SC, Laboratorio Nacional de Nanotecnología, Miguel de Cervantes 120, C. P. 31136 Chihuahua, Chih, Mexico

desired source materials. The main role of the vacuum is to maximize the mean free path of the vapor [20] and maintain purity of materials. On the other hand, literature survey shows that an appropriate route is the co-evaporation of the metal precursors followed by an heat treatment for sulfurization process [17].

This research is about deposition possibility of CZTS material by thermal evaporation starting from CuS, ZnS and SnS as precursors. The obtained material on transparent glass substrate was characterize its morphology, structure, elemental composition and optoelectronic properties.

2 Methodology

The films were deposited on a non-conductive glass substrate, it was cleaned by distilled water. The precursors were CuS (99%), ZnS (97%), and SnS (99%), they were provided by Sigma Aldrich, and the used quantity was stoichiometric to get CZTS. These precursors were ground in an agate mortar during 30 min. Then, it was mixture and place in a tungsten plate; in this step of the process the plate was heated and the mixed powder was evaporated. The pressure and electrical current for depositions were 4×10^{-5} Torr, and 180 A, respectively. Initially, the current was established at 120 A, and then it was raised with rate at 1 A/minute up to 180 A; the total time of deposition was an hour. After that, the films were annealed at 400 °C and 600 °C in a tubular furnace (Thermoline model 21100) equipped with Eurotherm 2116 temperature controller in an inert atmosphere, this heat treatment is carried out in order to reach a better crystallinity of the CZTS films. The tubular furnace was saturated with nitrogen atmosphere (0.5 atm.) and the sulfur atmosphere was set during the annealing with 0.25 g of solid sulfur. During the heat treatments, a temperature ramp was programmed at 10 °C per minute and it was for one hour.

The structural properties of the films were determined by Rigaku X-ray diffractometer, SmartLab model, using monochromatized Cu K α radiation ($\lambda = 1.54056$ Å). X-ray diffraction (XRD) patterns were collected over 2 h between 2 θ range from 20° to 60° using razing beam at 0.6° as a fix incidence angle. The Rietveld analysis was carried out using MAUD software v. 2.556. The Raman spectra were obtained using micro Raman Dilor LabRam, model II, with 632.8 nm laser wavelength.

The morphology of the films was studied using JEOL scan electron microscopy (SEM), model JSM-7100F, with EDS elemental analysis.

The thickness of the samples were measure by high sensitivity Profilometer Ambios XP-200, with a vertical range from 10 Å to 1.2 mm, with scanning length of 55 mm, using a needle with 2.5 μ m radius diamond tip, which was scanned along film surface with programmable positioning. The

roughness and the homogeneity in the films were observed with a Veeco Atomic Force Microscope Icon, with Asyst Scan. The obtained data were treated using the software NanoScope Analysis v. 1.5.

The measured absorbance spectra for each sample, were carried out using a Shimadzu UV-3101PC UV-VIS-NIR spectrophotometer, covering the wavelength range from 250 to 2500 nm. The bandgap value was determine from these data using Tauc equation:

$$\alpha = \frac{K(h\nu - E_g)^n}{h\nu}$$

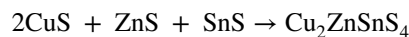
where α is the absorption coefficient, K is a constant, $h\nu$ is the photon energy, and n could be 0.5 or 2 depending on whether the transition band is indirect or direct, respectively. The optical band gap value was determined by the extrapolation of the straight-line plot of $(\alpha h\nu)^2$ vs. $h\nu$, considering that Kesterite has a direct band transition [21, 22].

The photoresponse of the films were obtained by an ohmic contact, for it was place two carbon electrodes ($\phi_C = 4.81$ eV) on the surface of the films ($\phi_{CZTS} = 4.6$ eV) in a surface area of 0.06 cm². The light source was incandescent tungsten halogen lamp with 100 W. A bias voltage of 0.1V was applied with a programmable Keithley voltage source model 619. To measure the response was used a Multimeter Keithley Model 230. The photoconductive measurements were carried out at 60 s; starting at 20 s in darkness, followed at 20 with illumination and finally at 20 s in darkness.

3 Results

3.1 Growing of the material

The films were successfully obtained on a non-conductive glass substrate, previously cleaned and the formation could be summarized according to the following reaction:



However, since the sulfide evaporates above 200 °C temperature, our samples were carried out at higher temperatures (400 and 600 °C). A sulfurization heating treatment process was made essential for our samples. This annealing process was carry out in a tubular furnace, the saturated sulfur atmosphere was created evaporating elemental S.

The characterization reports correspond to the films as deposited and annealed at 400 °C. Summary of the synthesis methodology is shown in Fig. 1 step by step.

Fig. 1 Methodology used in the synthesis of films, it includes: (1) substrate cleaning; (2) precursors milling (in stoichiometric quantities); (3) deposition (by thermal evaporation); (4) heat treatment after the deposition and (5) characterization techniques

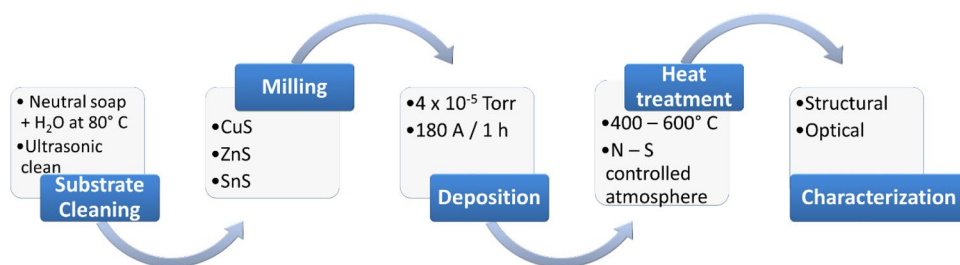
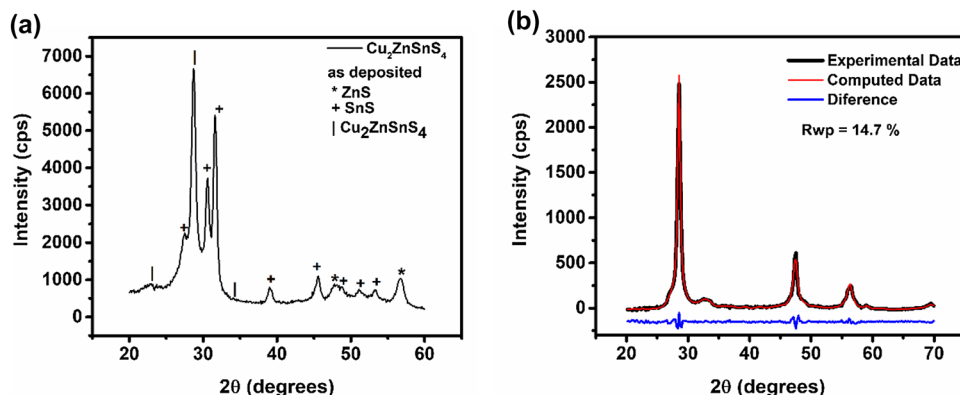


Fig. 2 **a** XRD for as deposited film; it shows the phases ZnS (*), SnS (+), and Cu₂ZnSnS₄ (l). **b** Final Rietveld profile refinement of the sample after annealing at 400 °C, the blue line is the result of the difference between the experimental data (black line) and the computed data (red line)



3.2 Structural determination

The structure was determined by XRD and Raman. Figure 2a shows a XRD patterns for as obtained film, the intensities located at 23.1°, 28.5°, and 32.9° are attributed to the diffraction direction of (110), (112), and (200) they belongs to d-spaces of kesterite phase Cu₂ZnSnS₄, (l; PDF 26–0575), respectively. However, in the same pattern it can be notice other lower intensities, which belong to ZnS (*; PDF 65–0309) and higher intensities of SnS (+; PDF 39–0354). The presence of these three phases corresponds to the powder precursors, which were used (milled) to the vapor deposition method for the synthesis of kesterite phase of CZTS. It means, just was deposited the precursors on the substrate, it is due to the temperature used to reach the complete precursors evaporation.

Figure 2b shows XRD pattern for the sample after heat treatment at 400 °C. The XRD intensities should be belongs to Cu₂ZnSnS₄ phase but it can be notice a decrease in the number of intensities (comparing to Fig. 2a), and this suggests that the number of phases decrease. However from the final plot, after Rietveld refinement procedure in order to get a good final refinement, it was consider two phases, kesterite CZTS (ICSD 171983) and ZnS (ICSD 15478), the presence of these phases content was estimated at 65% and 35% by refinement, respectively. A good fit was obtained with the I-42m and P3m1 space group, for CZTS and ZnS, respectively. The final refinement parameters for both samples are listed in the Table 1.

Table 1 Parameters obtained by Rietveld refinement for the sample annealed at 400 °C. A mix of phases was found and their respective values are listed

Parameters	Phase	
	CZTS	ZnS
Space group	I—42 m	P 3 m1
Cell lengths (Å)	a = 5.43 (1) b = 5.0 (1) c = 10.8 (5)	a = 3.84(4) b = 3.84(2) c = 62.9 (7)
Cell angle (°)	α = β = γ = 90	α = β = 90; γ = 120
Cell volume (Å ³)	293.22	803.64
Crystal size (nm)	127.6	17.7
Rwp (%)	14.7	

The heat treatment at 600 °C showed lost in the crystallinity of CZTS, and many impurities were detected, thus the stability of the crystal structure was lacke at this temperature (XRD pattern do not reported here).

The Raman spectra for study films are shown in the Fig. 3. The intensities for as deposited sample show a vibration mode at ν_1 (204 cm⁻¹), it indicates the presence of the SnS phase [23]. The values of the B(TO) and A modes are ν_2 (245 cm⁻¹) and ν_3 (285 cm⁻¹), respectively [24, 25]. These modes are mainly due to the vibrations associated with S and Zn/Sn, which represent Zn–S bonding states [26]. The ν_4 (317 cm⁻¹) is associated to the presence of ZnS. These vibration modes confirm the previous results found by XRD for this sample. In the case of the film obtained

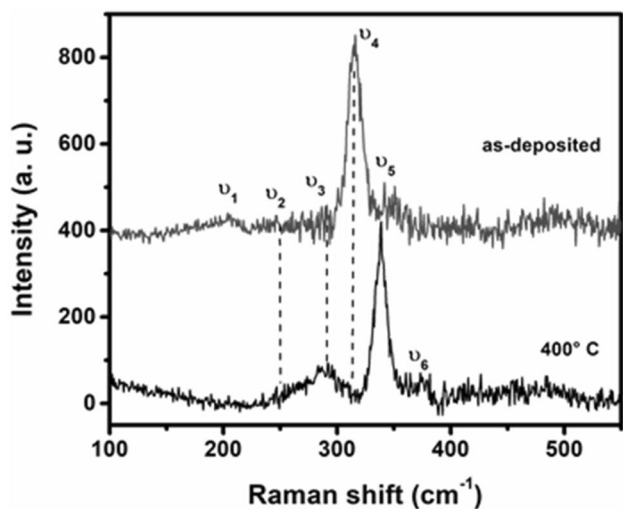


Fig. 3 Raman spectra for **a** as deposited and for **b** film after heat treatment at 400 °C, in both plots the vibration Raman are indicated

after heat treatment at 400 °C, it show strong intensity oscillation mode ν_5 (A_1 ; 334 cm^{-1}) and the weak mode ν_6 (E ; 368 cm^{-1}), these intensities belong to kesterite phase of CZTS [12, 13], this last ν_6 is associated with vibrations of S atoms [24, 27]. Then, Raman scattering analysis for annealed sample confirms the presence of these two phases, kesterite and ZnS, this secondary phase was found by Rietveld refinement of the XRD pattern (see Table 1). It can be corroborate the strong difference about intensity position and profile for both samples, in the case for as deposited film disappear the ν_4 oscillation but appear a strong ν_5 vibration after the heat treatment.

3.3 Surface morphology and elemental composition

The surface morphology was studied by SEM and AFM, and the elemental composition by EDS. Figure 4 show SEM images from surface and cross section for the annealed film. Figure 4a shows granular agglomerate of particles after annealed at 400 °C. It can be notice, the growth is homogeneously on the glass substrate, these agglomerate sizes are between 100 and 350 nm, and it can be notice some cracks, which are indicated with black arrows. This sample has about 900 nm of thickness, it can be observed from the corresponding cross-section image (Fig. 4b).

The elemental composition of this film after post-sulfurization at 400 °C was determined by EDS. According to its spectrum (Fig. 5), the semi-quantitative values are shown in Table 2. The ratio of $[\text{Cu}]/[\text{Zn}+\text{Sn}]$ is smaller (0.57) than the optimal ratio value, which should be between ~ 0.7 and

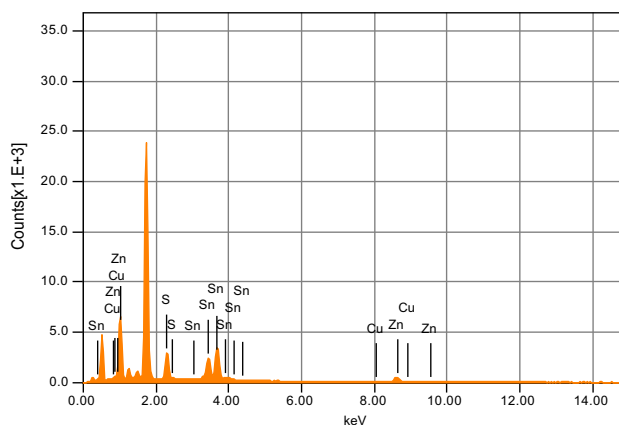


Fig. 5 EDS spectrum for film, after annealed at 400 °C. The presence of elements are identified

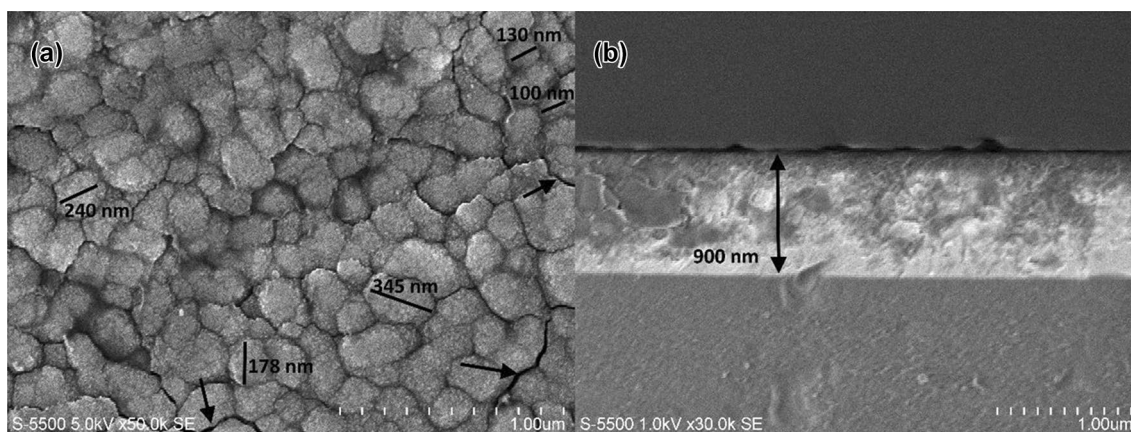


Fig. 4 SEM image for the film annealed at 400 °C. **a** Top view of the film shows an irregular surface, the agglomerate grain size is between 100 nm and 350 nm, some cracks in the film are indicated with arrows; **b** shows cross-section image, thickness is around 900 nm

Table 2 Elemental composition of annealed film at 400 °C

Element	Atomic %	[Cu]/[Zn+Sn]	Zn/Sn
S	2.19	0.57	2.32
Cu	16.41		
Zn	20.13		
Sn	8.66		

~0.9 [28, 29]. The content deviation of Cu from the desired composition is due to the re-evaporation of the mix powders during the thermal evaporation process [10].

The topographical image of both samples were studied by AFM. Figure 6a shows AFM 3D view image for the surface of as deposited film, from size $2 \times 2 \mu\text{m}$ scans. It can be observed the surface of it reveal a non-uniform morphology

with irregular shape. In the case of annealed sample, Fig. 6b from the same area shows bigger grain size, it increases due to the phase changes and heat treatment [25]. The roughness values were determined using Nanoscope software. These values were found 74.1 and 82.1 nm for as deposited and after annealing films, respectively. According to these values, roughness for annealed sample could be expected to increase but this behavior is due to the randomly oriented growth, during the heat treatment.

3.4 Optoelectronic properties

Optical transmittance and photoconductivity response were measure from the as deposited and after annealed samples. Figure 7 show the UV–VIS and near IR transmittance values. Figure 7a, b show that the optical response from as deposited

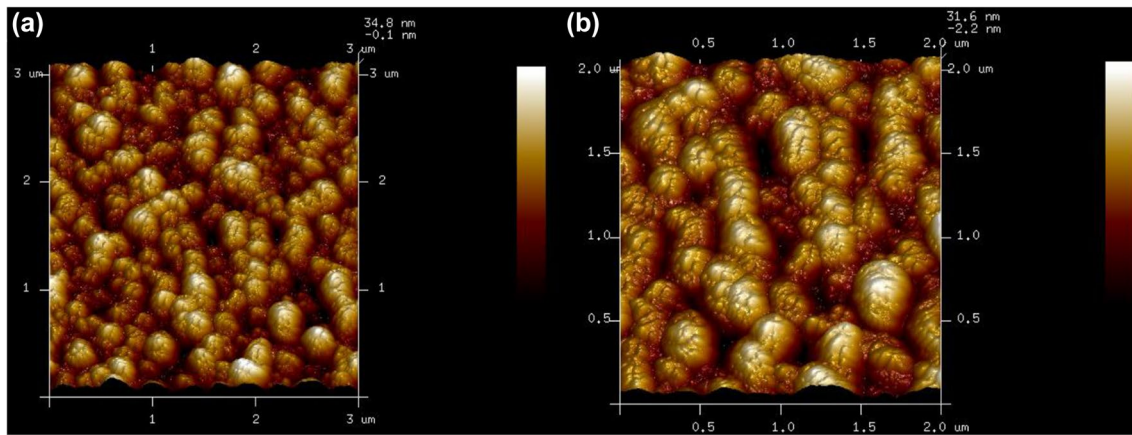


Fig. 6 AFM 3D image of the films **a** as deposited and **b** annealed at 400 °C

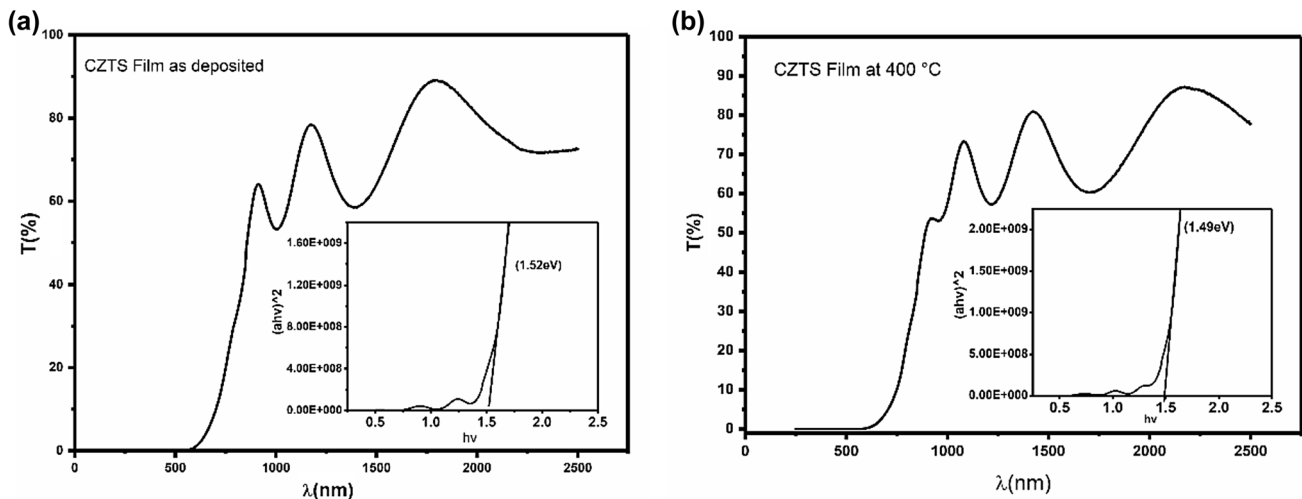


Fig. 7 a) UV–Vis transmission spectrum for films **a** as deposited and **b** annealed at 400 °C, the inset shows the extrapolation graph of $[(\alpha hv)^2$ vs. $hv]$

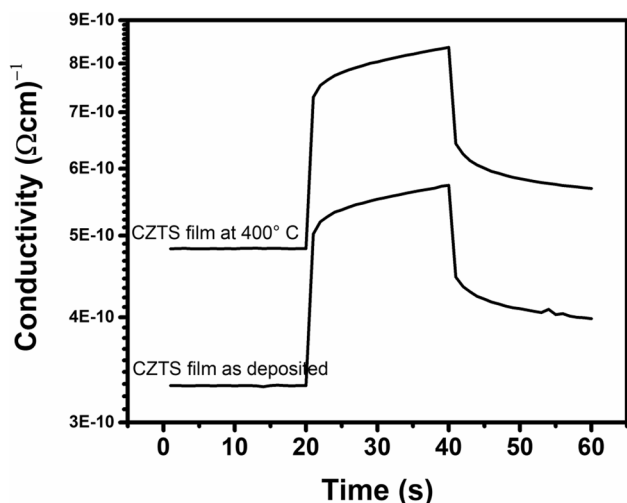


Fig. 8 Photoconductivity response of the films as deposited film and annealed at 400°C

and annealed films, respectively. They show average transmittance value around 78% for both samples, then these samples are transparent on this optical range (600–2500 nm) but highly absorbent in the visible range blue–green spectra (300–600 nm). From these data and the convenient method of plotting $(\alpha h\nu)^2$ vs. $h\nu$, the optical band gap values for both samples were estimated (see methodology). In the same figure the inset plot shows, the straight line whose intercept with the E axis for yields a direct band gap transition energy. The determined band gap values were 1.52 and 1.49 eV for as deposited and annealed sample, respectively. These values are in accordance with the literature [12].

Figure 8 shows the photoconductivity response values variation for as deposited and annealed sample. In this figure, it is possible to observe an immediately increase in the conductivity due to the light illumination. During the 20 s of irradiance, the conductivity decay slowly (saturate). The photosensitivity in the material is due to the charge carrier transport generated with the Photoelectric effect, and the slow decrease in conductivity value refers to the existence of strong trapping centers [21]. The conductivity increases in both samples but in the annealed sample is better due to the annealing process and the admix composition of Cu_2ZnSnS_4 and ZnS. The presence of ZnS in the film favors effective separations of photo generated electrons and holes through reducing lattices defects which acts as the recombination centers for charge carriers [30].

The photosensitivity was calculated using the expression [31]:

$$S = \frac{I_{light} - I_{dark}}{I_{light}}$$

where I_{dark} and I_{light} are the currents measured in the dark and light illumination, respectively. The calculated photosensitivity for as deposited and annealed sample were 0.69 and 0.72, respectively. Table 3 shows the values for the films, their conductivity, resistivity and photosensitivity. The measurement were carry out previously to the illumination (20 s), during illumination (20 s) and after illumination, these results are similar to previous works [31–33].

4 Conclusions

By thermal evaporation method was possible obtained admix of kesterite CZTS and ZnS phases content film. The elemental content ratio of $[Cu]/[Zn+Sn]$ after annealing is smaller than the optimal ratio, 0.57 but Rietveld refinement and Raman spectra analysis confirmed the presence of the kesterite CZTS and ZnS phases in the film.

The agglomerate grain size in the film was between 100 and 350 nm, some cracks were identified, and the thickness was estimated around 900 nm. The bandgap vales are 1.52 and 1.49 eV, for as deposited and annealed film, respectively. They showed photosensitivity around 0.69 and 0.72 for as deposited and annealed films. According to these results the films as obtained by this method could be used as absorber in the fabrication of solar cells. This admix compound is adequate for this porpoise because it present higher photoconductivity.

Table 3 Values of the resistivity, calculated from the conductivity (directly measured), the photosensitivity was calculated from the above expression

	20 (s) dark	20 (s) light	20 (s) dark
As deposited sample			
Conductivity ($\Omega\text{ cm}^{-1}$)	3.31E-10	5.61E-10	4.00E-10
Resistivity ($\Omega\text{ cm}^{-1}$)	3.02E+09	1.78E+09	2.50E+09
Photosensitivity (S)	0.697		
After heat treatment at 400 °C sample			
Conductivity ($\Omega\text{ cm}^{-1}$)	4.82E-10	8.36E-10	5.69E-10
Resistivity ($\Omega\text{ cm}^{-1}$)	2.07E+09	1.20E+09	1.76E+09
Photosensitivity	0.725		

Acknowledgements This research is financial supported by National Council of Science and Technology of Mexico and the Juarez Autonomous University of Tabasco, through the funds (CONACyT) SEP—CONACyT 239590 and PRODEP UJAT—PTC—253, respectively. The author thanks to M. C. Edith Ponce Recinos and M. C. Anabel González Díaz, by DRX and EDS-SEM measurements, respectively. In addition, the first author acknowledges to CONACyT for her graduate fellowship. Thanks to W. Antunez, E. Lestarjet and C. Ornelas for their help at Nanotech, CIMAV Chihuahua. Mexico.

References

1. K. Kaviyarasu, E. Manikandan, M. Maaza, *J. Alloys Compd.* **648**, 559 (2015)
2. K. Kaviyarasu, A. Ayeshamariam, E. Manikandan, J. Kennedy, R. Lachumananandasivam, U. Umbelino Gomes, M. Jayachandran, M. Maaza, *Mater. Sci. Eng. B* **210**, 1 (2016)
3. H. Krishna, R. Kalyanaraman, *Funct. Nanostruct.* pp. 65–106 (2008)
4. M. Kumar, U. Krishnan, P. Devi, A. Kumar, *J. Mater. Sci. Mater. Electron.* **29**, 10 (2018)
5. X. Lin, J. Kavalakkatt, M.C. Lux-Steiner, A. Ennaoui, *Adv. Sci.* **2**, 2 (2015)
6. M. Cao, L. Li, B.L. Zhang, J. Huang, L.J. Wang, Y. Shen, Y. Sun, J.C. Jiang, G.J. Hu, *Sol. Energy Mater. Sol. Cells* **117**, 81 (2013)
7. E. Kask, T. Raadik, M. Grossberg, R. Josepson, J. Krustok, *Energy Procedia* **10**, 261 (2011)
8. S.K. Wallace, D.B. Mitzi, A. Walsh, *ACS Energy Lett.* **2**, 776 (2017)
9. S.A. Vanalakar, G.L. Agawane, S.W. Shin, M.P. Suryawanshi, K.V. Gurav, K.S. Jeon, P.S. Patil, C.W. Jeong, J.Y. Kim, J.H. Kim, *J. Alloys Compd.* **619**, 109 (2015)
10. R.A. Wibowo, W.S. Kim, E.S. Lee, B. Munir, K.H. Kim, *J. Phys. Chem. Solids* **68**, 1908 (2007)
11. X. Lv, J.-Y. Wang, C. Zhu, Z. Wang, *Rare Met.* **35**, 718 (2016)
12. K. Loan, P. Thi, D. Anh, T. Nguyen, H. Ke, T. Quynh, A. Le, *J. Sol-Gel Sci. Technol.* 324 (2017)
13. P.R. Ghediya, T.K. Chaudhuri, *J. Mater. Sci. Mater. Electron.* **26**, 1908 (2015)
14. S. Mahjoubi, N. Bitri, H. Bouzouita, M. Abaab, I. Ly, *Appl. Phys. A* **123**, 452 (2017)
15. H. Guan, H. Shen, A. Raza, *Catal. Letters* **147**, 1844 (2017)
16. T.S. Tlemçani, E.B. Benamar, F.C. El Moursli, F. Hajji, Z. Edfouf, M. Taibi, H. Labrim, B. Belhorma, S. Aazou, G. Schmerber, K. Bouras, Z. Sekkat, A. Dinia, A. Ulyashin, A. Slaoui, M. Abd-Lefdil, *Energy Procedia* **84**, 127 (2015)
17. Y. Li, J. Chen, J. Ma, *J. Mater. Sci. Mater. Electron.* **26**, 6546 (2015)
18. C. Sripan, V.E. Madhavan, A.K. Viswanath, R. Ganesan, *Mater. Lett.* **189**, 110 (2017)
19. I. Lachebi, A. Fedala, T. Djenizian, T. Hadjersi, M. Kechouane, *Surf. Coatings Technol.* **343**, 160 (2018)
20. K. Priya, V.K. Ashith, G.K. Rao, G. Sanjeev, *Ceram. Int.* **43**, 0 (2017)
21. I.Montoya De Los Santos, M. Courel, N.R. Mathews, X. Mathew, *Mater. Sci. Semicond. Process.* **68**, 68 (2017)
22. M.B. Dergacheva, K.A. Urazov, A.E. Nurtazina, *Russ. J. Electrochem.* **53**, 324 (2017)
23. I.G. Orletskii, M.N. Solovan, F. Pinna, G. Cicero, P.D. Mar'yanchuk, E.V. Maistruk, E. Tresso, *Phys. Solid State* **59**, 801 (2017)
24. D. Dumcenco, Y.-S. Huang, *Opt. Mater. (Amst.)* **35**, 419 (2013)
25. L. Chen, C. Park, *Korean J. Chem. Eng.* **34**, 1187 (2017)
26. P.K. Sarswat, M.L. Free, *J. Mater. Sci.* **50**, 1613 (2015)
27. T.T.T. Nguyen, H. Shin, G.Y. Kim, J.R. Kim, W. Jo, S. Yoon, K.D. Lee, J.Y. Kim, *J. Korean Phys. Soc.* **66**, 117 (2015)
28. Y. Zeng, G. Liang, P. Fan, Y. Xie, B. Fan, J. Hu, *J. Mater. Sci. Mater. Electron.* **0**, 0 (2017)
29. D.B. Mitzi, O. Gunawan, T.K. Todorov, K. Wang, S. Guha, *Sol. Energy Mater. Sol. Cells* **95**, 1421 (2011)
30. X. Xu, L. Hu, N. Gao, S. Liu, S. Wageh, A.A. Al-Ghamdi, A. Alshahrie, X. Fang, *Adv. Funct. Mater.* **25**, 445 (2015)
31. J. Henry, K. Mohanraj, G. Sivakumar, *Optik (Stuttg.)* **141**, 139 (2017)
32. Y. Wang, Y. Huang, A.Y.S. Lee, C.F. Wang, H. Gong, *J. Alloys Compd.* **539**, 237 (2012)
33. K.S. Gour, B. Bhattacharyya, O.P. Singh, A.K. Yadav, S. Husale, V.N. Singh, *J. Alloys Compd.* **735**, 285 (2018)

Publisher's Note Springer Nature remains neutral with regard to jurisdictional claims in published maps and institutional affiliations.